INSTITUTE OF PHYSICS PUBLISHING PLASMA PHYSICS AND CONTROLLED FUSION

Plasma Phys. Control. Fusion **44** (2002) R1–R26 PII: S0741-3335(02)17001-1

**REVIEW ARTICLE**

# Dynamical processes in complex plasmas

**A Piel and A Melzer**

Institut für Experimentelle und Angewandte Physik, Christian-Albrechts-Universität Kiel, Kiel D-24098, Germany

E-mail: piel@physik.uni-kiel.de

Received 3 September 2001
Published 14 December 2001
Online at stacks.iop.org/PPCF/44/R1

**Abstract**

In this review, a systematic overview of dynamical processes in complex (dusty) plasmas is given. Complex plasmas consist of electrons, ions, neutrals, and microparticles of nanometre to micrometre size, which are responsible for the unusual properties of this kind of plasmas, such as the formation of liquid or solid phases at strong electrostatic coupling. The examples represent the progress in this field within the last five years and mostly such cases were chosen, in which experimental results could be compared with theory or where the phenomenon has a diagnostic application. The presentation begins with single particle effects, where levitation, confinement in plasma traps, charging, and oscillations are involved. It is shown that vertical oscillations can be used for particle charge measurements. Nonlinear and parametric effects as well as self-excited oscillations are discussed. Then the interaction force between the particulates is explored in few-particle systems. Scattering experiments show that the interaction in the levitation plane can be described by shielded Yukawa-type potentials, while the vertical interaction is governed by additional attractive wake fields. The latter are shown to be asymmetric and lead to the formation of vertical strings. The normal modes of one-dimensional or two-dimensional particle arrangements are useful tools for diagnostics. Many-particle effects are discussed in terms of low-frequency electrostatic waves. The dust-acoustic wave, the dust ion-acoustic wave, and two types of dust lattice waves (shear and compressional) are discussed with respect to diagnostic applications, among them Mach cones in plasma crystals. Laser methods are now established for the excitation of such modes. Two novel types of instabilities, the wake-field instability and the void-forming instability, as well as first results on dust ion-acoustic shocks are presented.

## 1. Introduction

Complex plasmas are gas plasmas consisting of electrons, ions, and neutral atoms that additionally contain microscopic particles with sizes ranging from 10 nm to some 10 $\mu$m.

  

This state of matter is ubiquitous in space, e.g. in the interplanetary medium, in interstellar clouds, in comet tails, and in the ring systems of the giant planets as well as in mesospheric noctilucent clouds [1, 2]. In microchip manufacturing, avoiding particle contamination during the many production steps that involve plasmas is a technological challenge [3, 4]. On the other hand, the growth, transport, and deposition of nanoparticles is the central goal of many plasma deposition techniques, e.g. in the manufacturing of amorphous solar cells [5–8]. Since the early 1990s, research in complex plasmas is rapidly evolving. The original name *dusty plasmas* is nowadays replaced by *complex plasmas* in analogy to *complex fluids* to emphasize many fundamentally different properties of this medium that distinguish it from ordinary gas plasmas. The field of complex plasmas is now maturing and the interested reader can find timely monographs, e.g. on dusty plasmas in space [9], technological applications [10], or on waves in dusty space plasmas [11]. Recent surveys on subtopics cover dust phenomena in processing plasmas [12], waves and instabilities in dusty plasmas [13], laser excited waves in plasma crystals [14, 15], solid and liquid phases in dusty plasmas [16–18], magnetic field effects [19], diagnostical aspects [20], and collective processes in dusty plasmas [21, 22].

The microparticles in complex plasmas are electrically charged by collection of plasma electrons and ions as well as by photoemission or secondary electron emission [1, 2]. In laboratory plasmas usually the collection processes dominate and the particles attain a high negative charge. In space, photoemission and secondary emission become more important, and either reduce the negative charge or even lead to positively charged particles. Complex plasmas with nanometre-sized particles, to some extent, behave like negative ion containing plasmas, in that a part of the negative electron charge is bound to heavier particles, which affects the mobility and the contribution to shielding by negative charges. Unlike negative ions, the charge of the microparticles is not fixed but becomes itself a dynamical variable, which introduces many new phenomena, such as a novel type of wave damping [23, 24] and an inherent nonlinearity of the electric field force.

Most ordinary plasmas in space and laboratory are weakly coupled, which means that the interaction energy of nearest neighbours is much smaller than their thermal energy. This situation reverses in complex plasmas with micrometre-sized particles which then become strongly coupled: the negative charge can become so large (typically $10\,000e$) that the interaction energy of nearest neighbours exceeds their thermal energy. A consequence of strong coupling is the formation of liquid or solid phases. Ordered solid phases were predicted by Ikezi [25] and observed as *plasma crystals* [26–29]. Much experimental [30–37] and theoretical work [38–48] was devoted to study the structure and the order–disorder phase transition of the plasma crystal, which may serve as a macroscopic model system for melting in two or three dimensions. The dynamical and thermodynamic properties of the particle system can be conveniently studied with video cameras at a kinetic level.

Despite the high electric charge on larger microparticles, the charge-to-mass ratio is always very small compared to that of the ions, not to mention electrons. Hence, the dynamic response of these particles is expected to give rise to many new wave phenomena at very low frequencies, such as the dust-acoustic wave (DAW) [49–54] or the dust lattice wave (DLW) [55].

The particles in complex plasmas are subject to a variety of forces, which are mostly considered unimportant in ordinary plasmas. Because of their high mass compared to the ion mass, the gravitational force becomes dominant. This leads, for example, to sedimentation of charged dust in laboratory devices. Electric field forces are known to be the most important forces in ordinary gas plasmas. In complex plasmas, they can become even more effective, e.g. when the high charge on micrometre-sized particles leads to the pick-up of considerable energy even in weak dc or low-frequency electric fields. Friction of the particles with the residual neutral gas [56] has a damping influence on waves and oscillations. On the other

hand, collisions with neutral particles can also exert drag forces from streaming neutral gas and thermophoretic forces in the presence of temperature gradients. Ion drag forces are determined by momentum transfer in the process of charge collection and in Coulomb scattering of ions by the highly charged particles. These forces have different dependencies on the particle radius [2] and thus their relative importance varies with particle size.

This review is intended to survey the advances during the last five years in the field of low-frequency oscillations, waves, and more advanced dynamical phenomena in complex plasmas. As examples mostly such situations are selected, where theories could be experimentally tested. Many of these phenomena are relevant for the determination of fundamental properties of complex plasmas, such as the particle charge, the interaction law, shielding effects, or the confinement of complex plasmas. On the other hand, some surprising properties of complex plasmas are described, like attractive forces between like charges, which arise from wake potentials and determine structure and stability of plasma crystals.

## 2. Charging, confinement, and oscillations of single particles

### *2.1. Charging of microparticles*

When secondary emission and photoemission can be neglected, an isolated microparticle in a plasma environment behaves much in the same way as a floating probe. Because of the higher electron mobility, the particles attain a negative floating potential $\phi_p$ that is determined by a balance of electron repulsion and ion collection $I_e + I_i = 0$. The electron current is given by

$$I_e = -4\pi a^2 e n_e \left(\frac{k_B T_e}{2\pi m_e}\right)^{1/2} \exp\left(\frac{e\phi_p}{k_B T_e}\right), \tag{1}$$

where $m_e$, $n_e$, and $T_e$ are the electron mass, density, and temperature. $a$ is the radius of the assumed spherical particle. The ion current to the grain is usually approximated by the 'orbital motion limit' (OML) model for a spherical probe [57, 58].

$$I_i = 4\pi a^2 n_i e \left(\frac{k_B T_i}{2\pi m_i}\right)^{1/2} \left(1 - \frac{e\phi_p}{k_B T_i}\right). \tag{2}$$

Here, $m_i$, $n_i$, and $T_i$ are the ion mass, density, and temperature. The OML model is applicable as long as the particle radius is small compared to the Debye length, $a \ll \lambda_D$ [59, 60]. In situations with streaming ions, the ion temperature has to be replaced by the kinetic energy of the ions [61, 62]. For the special case of an isothermal hydrogen plasma, the particle's floating potential approaches the classical Spitzer value $\phi_p = -2.51\, kT_e/e$ [63]. In laboratory plasmas, mostly $T_e \gg T_i$, and usually heavier ions (e.g. argon) are used. Some values of the normalized floating potential $\eta_p = e\phi_p/k_B T_e$ in non-isothermal hydrogen and argon discharges are compiled in table 1.

An increase of the ion current can be expected from trapped ion effects [64]. In astrophysical situations, electron emission by the photoeffect or by the impact of energetic particles has to be taken additionally into account [65]. Because the secondary emission yield

**Table 1.** Normalized floating potential $\eta_p = e\phi_p/k_B T_e$ in non-isothermal hydrogen and argon plasmas.

| $T_e/T_i$ | 1 | 2 | 5 | 10 | 20 | 50 | 100 |
|---|---|---|---|---|---|---|---|
| $H^+$ | −2.504 | −2.360 | −2.114 | −1.909 | −1.700 | −1.430 | −1.236 |
| $Ar^+$ | −3.994 | −3.798 | −3.491 | −3.244 | −2.992 | −2.660 | −2.414 |

is a non-monotonous function of ion energy, the particle potential can be multivalued when secondary emission becomes important [66].

The surface charge $Q_d$ on this particle can be obtained from the capacitance model [67], $Q_d = C\phi_p$, in which an isolated grain is considered as a spherical capacitor. In vacuum the capacitance is $C = 4\pi\epsilon_0 a$. The polarization of the plasma increases the capacitance to $C = 4\pi\epsilon_0 a(1 + a/\lambda_D)$, which for $a \ll \lambda_D$ reduces to the vacuum value.

When the dust grains (of density $n_d$) are densely packed and their interparticle distance $b$ becomes smaller than the Debye length $\lambda_D$, the charge $Q_d$ on the neighbouring particles affects the quasineutrality of the plasma, $n_i e = n_e e + n_d|Q_d|$, which results in a depletion of the free electron density. Further, this leads to a reduced electron charging current and eventually to a reduction of the grain potential with respect to the plasma potential in the dust cloud [68, 69]. This effect becomes important, when the parameter $P = (n_d Q_d/n_0 e) = 695(T_e, \text{eV})(a, \mu\text{m})\, n_d/n_0 > 0.1$. Here $n_0$ is the plasma density outside of the dust cloud.

The charge of dust particles was originally measured by extracting dust particles from the plasma [70–72]. While this technique is the most direct, there may be some ambiguities concerning a charge variation during the passage through the plasma boundary sheath. Barkan *et al* [73] used the change in the ratio of electron to ion saturation current of a Langmuir probe as a measure for the average bound charge on the dust grain.

### *2.2. Charging as a stochastic process*

The discreteness of the elementary charge causes distinct differences from the continuous charging model discussed so far. From a simulation of the charging process, Cui and Goree [74] obtained the power spectrum and the charge distribution function for the random charging process. They pointed out that a charged particle with average charge number $Z = Q_d/e$ has an RMS fluctuation of the charge $\delta Z^{\text{RMS}} = \eta\langle Z\rangle^{1/2}$ with $\eta = 0.5$. This makes charge fluctuations most important for nanometre-sized grains, where the charge can even fluctuate between positive and negative, which facilitates the coagulation of particles (see e.g. [7]). This result was confirmed with analytic methods by Matsoukas *et al* [75] and later extended [76] to situations with directed ion flow. Analytical expressions for the charge distribution function were given by Gordiets and Ferreira [77, 78]. Khrapak *et al* [79] give $\eta$-values between 0.46 and 0.61, which depend weakly on $T_e$ and on atomic mass number of the ion, whereas the charging frequency is a sensitive function of these parameters.

According to various theoretical models, dust charge fluctuations play an important role in the random excitation of waves [80] and in the destabilization of DAWs [81,82]. Unfortunately, experimental investigations on these aspects are still lacking.

### *2.3. Levitation and harmonic oscillations*

In many laboratory experiments, clouds of micrometre-sized particles are trapped in an ion sheath between the plasma and an electrode. Such a situation is found in capacitively coupled radiofrequency (rf) discharges between parallel plates that are typically operated at 13.56 MHz. While the electrons follow the rf electric field, the ions and microparticles, because of their large inertia, are only reacting to the time-averaged field, which generates the levitating electric force. The distribution of the net ion space charge in the sheath is sufficiently homogeneous, which implies that the electric field increases nearly linearly from the plasma edge to the electrode [83–85].

Melzer *et al* [29] noticed that the linear increase of the electric field in the sheath leads to vertical confinement of the microparticles in an effective parabolic potential energy well

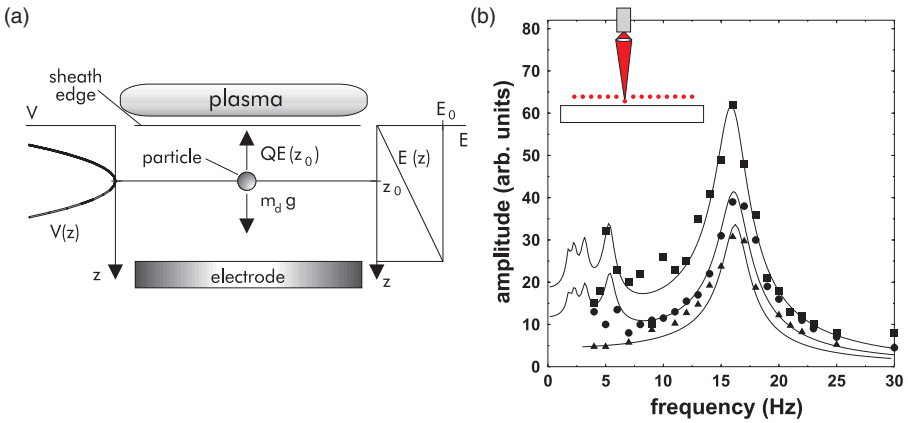


**Figure 1.** (*a*) Confinement of a dust particle in a harmonic potential energy well due to the linear increase of the sheath electric field. (*b*) Resonance curves for vertical oscillation excited with radiation pressure from a chopped laser (inset) or electrode bias. Triangle: electrode excitation with sine wave; square: laser excitation with square wave; circle: electrode excitation with square wave (from [86]).

(figure 1(*a*)), $V(z) = \frac{1}{2}M_{\rm d}\omega_0^2(z-z_0)^2$. This potential well possesses a unique natural frequency of oscillation

$$\omega_0 = \left(\frac{Q_{\rm d}}{M_{\rm d}}\frac{n_{\rm i}e}{\epsilon_0}\right)^{1/2}, \tag{3}$$

which is determined by the charge-to-mass ratio, $Q_{\rm d}/M_{\rm d}$, of the dust grains and the ion density $n_{\rm i}$ in the sheath. The latter can be measured with probes in the plasma close to the sheath. Corrections for the density reduction in the sheath as well as for the time-averaged neutralization by electrons in the sheath can be applied [87]. Vertical oscillations of the microparticles are stimulated by applying an additional, low-frequency sinusoidal bias voltage to the lower electrode. As a function of the excitation frequency, a pronounced resonance is found, which is broadened by friction with the neutral gas.

Using monodisperse polymer particles with a well-defined mass $M_{\rm d}$, accurate charge measurements became possible [87]. This technique was later refined by Homann *et al* [86] by stimulating the vertical resonance of a single particle with a focused laser beam ($\lambda = 690$ m; 40 mW) instead of forcing all suspended particles with electrode bias. The laser is chopped at frequencies between 1 and 30 Hz. Figure 1(*a*) shows the experimental arrangement. The corresponding resonance curves for laser excitation and for applying a low-frequency bias to the electrode are shown in figure 1(*b*). The resonance occurs at $f_{\rm res} = \omega_0/2\pi = 16$ Hz and the width of the resonance curve corresponds to an Epstein friction coefficient of $\beta = 17.4\,{\rm s}^{-1}$. The resonance frequencies for both kinds of excitation agree very closely and confirm the earlier measurements [87].

Spurious resonances at $f_{\rm res}/3$ and at $f_{\rm res}/5$ found with laser excitation can be attributed to the excitation of the fundamental resonance by odd harmonics in the exciting square wave signal. The same spurious resonances appear, when the electrode is biased with a square wave signal. The resulting charge on a particle of 9.47 $\mu$m diameter is $Q_{\rm d} = -8300e$ at 70 Pa and shows a general tendency to rise for decreasing gas pressure to reach $-12\,000e$ at 30 Pa [31].

A variant of the resonance technique was recently used by Tomme *et al* [84,85] to explore the electric field distribution in the sheath. There, a single particle is dropped into the plasma, where it performs a damped oscillation and becomes trapped in the sheath. From the full particle

trajectory, the particle charge and the friction coefficient can be extracted. For particles of 5 $\mu$m radius, charge values of $Q_d = -6000e$ to $-11\,000e$ were reported, depending on the discharge conditions. Using particles of different size, the entire sheath region could be explored and the parabolic shape of the (time-averaged) electric potential was verified. The resonance method was compared with the evaluation of the equilibrium force balance in the experiments of Arnas *et al* [88].

Fortov *et al* [89] have used the local electric field in standing striations of a dc discharge to levitate and trap a cloud of dust particles. It was found that ordered structures form, which confirm the strong coupling between the dust grains. Thomas and Watson [90] report dust confinement in an anode double layer.

### *2.4. Nonlinear oscillations*

At large amplitudes, the vertical oscillations are no longer described by a parabolic confining potential energy well. Two kinds of nonlinearities can be expected in this case: first, a deviation from the linear increase of the electric field with distance from the sheath edge, second, a dependence of the particle charge on position. Both aspects have been studied in recent experiments. Large amplitude oscillations were excited with a sinusoidal bias voltage that, in the experiment of Ivlev *et al* [91], was applied to a wire immediately below the particle. Zafiu *et al* [92] applied the bias to the lower electrode. In both cases nonlinear resonance curves were observed, in which the nonlinear resonance shifts to lower frequencies (see figure 2(*a*)). The nonlinear resonance curves show characteristic jumps at critical frequencies that depend on the way of approach (decreasing or increasing exciter frequency). Because of these jumps the nonlinear resonance curves show pronounced hysteresis. The nonlinear resonance curves can be analysed by comparing with numerical integrations of the nonlinear equation of motion

$$\ddot{z} + \beta\dot{z} + C_1 z + C_2 z^2 + C_3 z^3 + \cdots = \frac{F_{\text{ext}}}{M_d}\cos(\omega t). \tag{4}$$

For $C_2 = C_3 = 0$, the coefficient $C_1 = \omega_0^2$ gives the linear resonance frequency. $z = 0$ refers to the equilibrium position of the particle. If we expand the electric field and the particle charge into a power series ($E(z) = E_0 + E_1 z + E_2 z^2 + E_3 z^3$, $Q(z) = Q_0 + Q_1 z + Q_2 z^2 + Q_3 z^3$), we

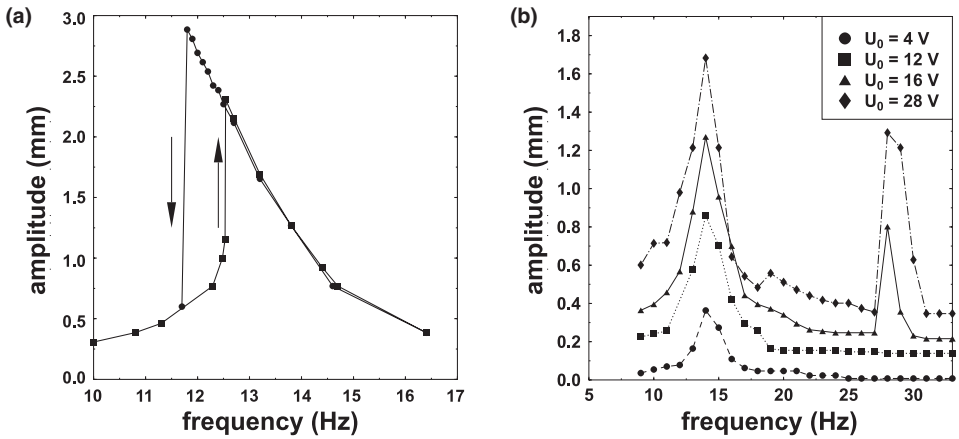


**Figure 2.** (*a*) Nonlinear resonance curve (from [92]). (*b*) Parametric excitation of the plasma trap with a probe (from [93]). Above a threshold voltage, the vertical oscillation is excited with a signal at twice the natural frequency ($2f_0 = 28$ Hz).

obtain: $C_1 = (Q_0E_1+Q_1E_0)/M_d$; $C_2 = (Q_0E_2+Q_1E_1+Q_2E_0)/M_d$; $C_3 = (Q_0E_3+Q_1E_2+Q_2E_1+Q_3E_0)/M_d$. $C_2$ describes the up/down asymmetry of the potential in the sheath and $C_3$ the softening or hardening of the potential energy well at large amplitudes. Comparing the measured nonlinear resonance curve with theoretical curves obtained by numerical integration of the equation of motion (4), the coefficients $C_1$–$C_3$ are determined, from which the nonlinearities in the electric fields ($E_1$–$E_3$) and/or the position dependence of the charges ($Q_0$–$Q_3$) have been extracted [91,92]. The magnitude of the charge $|Q_d|$ is found to decrease towards the electrode, which is attributed to a reduction of the electron charging current.

### *2.5. Parametric excitation of the trap*

Schollmeyer *et al* [93] noticed earlier that a biased probe wire in the sheath region for the excitation of particle motion leads to a distortion of the confining plasma trap. This, in turn, gives rise to parametric excitation of the vertical resonance, e.g. when the probe is biased with a signal at twice the natural resonance frequency $\omega_0$. The parametric nature of this excitation could be clearly demonstrated by the presence of a threshold amplitude which increased with the frictional damping of the system (see figure 2(*b*)). The observation of nonlinear resonances at $\frac{1}{2}\omega_0$ and at $2\omega_0$ in the experiments of Ivlev *et al* [91] was also accompanied by a threshold value, which hints at parametric excitation in this case, too.

### *2.6. Self-excited vertical oscillations*

Nunomura *et al* [94] found that the equilibrium position of a microparticle levitated in the space charge sheath of a biased plate in a dc plasma becomes unstable under certain conditions. Spontaneous vertical oscillations (near $\omega_0$) set in when the gas pressure is decreased below a critical value (approximately 0.4 Pa, argon) and the plasma density is low ($n_e < 3 \times 10^{14}\,\mathrm{m}^{-3}$). It is argued that the particle can gain energy in the sheath by a position-dependent charge and a delayed charging mechanism: the particle gains energy if the charge while moving down in the electrostatic potential is more negative than the charge while the particle moves upwards. This instability was studied theoretically in more detail by Ivlev *et al* [95] and Shukla [96]. The condition for instability $E_0\partial Q_0/\partial z < 0$ was originally introduced by Nitter [97] in a slightly different notation. Takamura *et al* [98] have reanalysed the delayed charging mechanism for the transverse DLW (see section 4.4). In the limit of long wavelength, this wave mode describes vertical oscillations. The criterion for unstable waves $(\tau_c/M_d)|E_0\partial Q_0/\partial z| > \beta$ ($\tau_c$ is the charging time) is the same as for unstable vertical oscillations [91]. Agreement with experiments could be achieved, when the presence of a small (2%) population of hot electrons is postulated, which has a substantial effect on the particle charge variation $\partial Q_0/\partial z$ in the sheath. This type of instability was mostly observed in dc discharges while it was only reported for one case of rf discharge [99].

### *2.7. Horizontal confinement*

The particle clouds that sediment towards the lower electrode in typical rf discharges require a lateral confinement to prevent the unrestricted radial expansion under the mutual repulsion of the particles. Here one can distinguish two types of confinement. In 'surface confinement', a flat metal ring on the electrode [87] or a depression of the electrode surface [53] is used to raise the equipotentials at the boundary of the cloud and to produce a localized radial electric field that balances the electrostatic pressure of the cloud. In 'volume confinement', a shaped electrode is used to produce a parabolic confining potential well $W_{pot}(r) = \frac{1}{2}\gamma r^2$. In the

latter case, the confinement parameter $\gamma$ can easily be determined from sloshing oscillations at the natural frequency $\omega_s = (\gamma/M_d)^{1/2}$ of this potential well (e.g. in particle collision experiments [100, 101]). Elongated particle traps [102, 103] were used to form linear chains of particles for experiments with linear chains of particles. Besides using the distortion of the equipotentials for particle confinement, it is also well known [3, 104] that the discharge mechanism of an rf discharge can form regions of enhanced positive plasma potential above sharp edges of the electrode, in which negative microparticles are trapped. Similarly, particles can be confined above grooves of a few millimetres depth and width [105].

### *2.8. Surface charge dipoles*

Inhomogeneous charge distributions on the surface of the microparticles were originally discussed in connection with the formation of electric dipoles that could lead to additional attractive forces, for instance in the coagulation process of dust particles [106]. The surface charge distribution for a dielectric particle in a directed (supersonic) ion flow was calculated with particle-in-cell simulations [107, 108] and with analytical methods [109]. Ivlev *et al* [110] note that the dipolar charge distribution leads to particle rotation. The role of dipole–dipole interaction for the alignment of particles was discussed [111] in order to explain experimental results with elongated particles [112], in which the particle size was comparable with the Debye length. This suggested alignment process is different from the presently favoured view of wake-field formation [40, 43, 113] as the dominant attractive force that determines the vertical alignment in multilayer plasma crystals.

The role of inhomogeneous charge distribution becomes even more important for rod-shaped objects. Annaratone *et al* [114] have studied the suspension of short nylon threads in the sheath of an rf discharge. Rods below a critical length are found to be levitated vertically. Horizontally levitated rods are found at two different equilibrium heights in the sheath. Inclined rods exhibit a characteristic spinning motion about the vertical direction. Most of these observed features can be explained by a charging model based on the radial motion theory [115] and the resulting forces in a sheath with a parabolic potential. Tskhakaya and Shukla [116] give a model for quivering and bouncing motion of elongated dust grains.

### *2.9. Positively charged microparticles*

While positively charged microparticles by photo or secondary emission are the most common state in space [65], laboratory investigations of positively charged particle systems are still in their infancy. A thorough theoretical analysis of UV-induced particle charging and of the conditions for Coulomb crystallization was given by Rosenberg *et al* [117, 118]. Other recent theoretical work was devoted to the formation of positively charged grains in mesospheric noctilucent clouds by solar UV radiation [119]. The field of positively charged particles in laboratory plasmas has many similarities with the problem of current collection by positively charged spacecrafts and tethers in the near-earth environment [120, 121], although the situation there is even more complicated by the presence of a magnetic field. Likewise, probe theory for magnetized plasmas has obtained new incentives from models for spacecraft charging [122].

A fundamental experimental study of photoelectric charging of small dust grains in a vacuum chamber was recently reported by Sickafoose *et al* [123]. The charge on the particle, measured with a Faraday cup, was found to scale with $hc/\lambda - W$ ($\lambda$ being the UV wavelength and $W$ the workfunction). Particles of about 50 $\mu$m radius were found to carry $5 \times 10^4$ elementary charges. A net positive charging of glass microballoons was reported by Samarian and Vaulina [124] from a plasma discharge in air. The positive charge, which is attributed to

the UV resonance radiation of nitrogen at a photon energy of 8.2 eV, becomes evident from the reversed electric field that levitates the particles. However, there are still many unknown parameters in these peculiar systems, like the density and energy distribution of free electrons, which is strongly affected by the formation of negative ions in electronegative gases. The free electrons determine competing processes for particle charging, namely the negative charging flux to the particle as well as the excitation of UV resonance radiation that discharges the particles.

## 3. Few-particle systems and interparticle forces

The forces acting between the charged microparticles can be determined from their equilibrium positions in a particle arrangement or from the elastic properties that result from their interaction forces. The average interparticle potential is often assumed to be isotropic and purely repulsive and is approximated by a shielded (Yukawa-type) potential

$$\Phi(r) = \frac{Q_\mathrm{d}}{4\pi\epsilon_0 r} \exp\left(\frac{-r}{\lambda_\mathrm{D}}\right). \tag{5}$$

The assumption of isotropy is certainly not appropriate in the space charge sheath, which is permeated by a supersonic ion flow, but experiments show that it is still a reasonable approximation in the horizontal plane. In the vertical direction, accumulation of positive space charge in the wake of a particle creates an additional attractive force [40, 125, 126], as will be shown below. From linear response theory, the Yukawa-type potential in the horizontal plane is confirmed [60].

Excitation of coupled oscillations or waves in small Coulomb or in extended plasma crystals can be used to determine the two unknowns of the Yukawa potential, namely the particle charge $Q_\mathrm{d}$ and the shielding length $\lambda_\mathrm{D}$. In this section, we first discuss the interaction of particles in the horizontal plane, then turn to vertical interaction in the sheath environment, and finally comment on diagnostic methods based on particle interactions.

### *3.1. Scattering experiments*

The most direct exploration of the interparticle potential over a wide range of interparticle distance was achieved in the two-particle scattering experiments of Konopka *et al* [101]. The authors use the technique of head-on collisions of two particles that are confined in the sheath of an rf discharge and are subject to lateral confinement by a parabolic potential well. In earlier experiments of the same authors [100], it was demonstrated that the analysis of the particle trajectories in terms of Yukawa potentials leads to agreement of the particle charge with the vertical resonance method [29]. While in the earlier experiments both particles were released from two positively biased Langmuir probe tips on opposite sides of the lateral confinement region, the technique was later refined to have one particle at rest in the centre of the trap and releasing the other particle from an arbitrary position in the trap [101].

The data analysis takes into account the lateral parabolic confinement, which is characterized by the sloshing frequency $\omega_\mathrm{s}$. Since the particle motion is subject to friction with the neutral gas, particular care has to be taken to correct for frictional losses. The damping constant can be experimentally determined by analysing the centre of mass motion of the two-particle system, which is well approximated by a damped harmonic oscillator. The interparticle potential energy at a particle separation $d$ then becomes

$$W_\mathrm{pot}(d) = -\frac{M_\mathrm{d}}{4}\dot{d}^2 - \frac{1}{2}M_\mathrm{d}^2\omega_\mathrm{s}^2 d^2 - \frac{\beta}{2}\int_{t_0}^{t(d)} \dot{d}^2 \,\mathrm{d}t'. \tag{6}$$

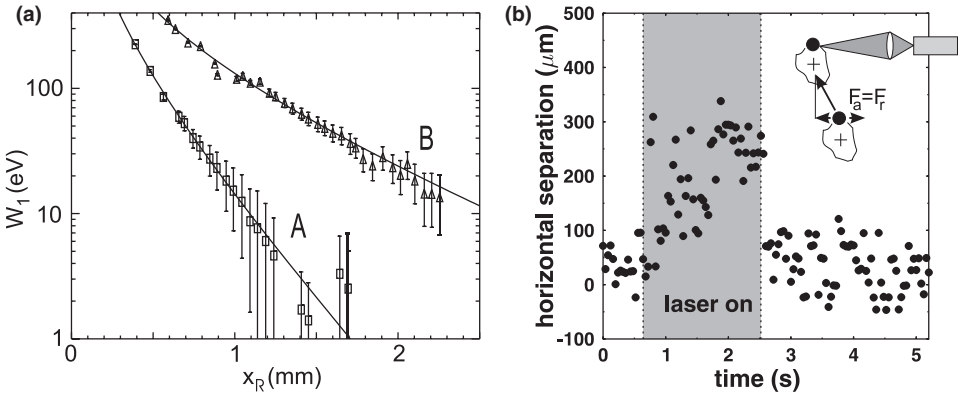


**Figure 3.** (*a*) Resulting interparticle potential from the binary collision experiments of Konopka *et al* with fitted Yukawa potentials [101] (A: $U_{pp} = 233$ V, B: $U_{pp} = 64$ V). (*b*) Experimental verification of wake-field attraction. During the 'laser on' phase the lower particle lags behind the upper (inset) due to friction with the neutral gas (from [127]).

The resulting potential energy curve can be approximated by a Yukawa potential in the investigated range 0.3 mm $< d <$ 2.2 mm. The shielding parameter was varied by decreasing the rf voltage applied to the discharge, which mostly affects the electron density. Consequently, the particle charge was found in a narrow range $Q_d = 13\,900e$ (at $U_{pp} = 233$ V, $T_e = 2.0$ eV) to $Q_d = 17\,100e$ (at $U_{pp} = 64$ V, $T_e = 2.8$ eV), while the shielding length increased from $\lambda_D = 0.34$ mm (curve A in figure 3(*a*)) to 0.78 mm (curve B). The resulting particle charge agrees with earlier measurements at the low pressure of 2.7 Pa (argon).

The collision experiments did not give evidence for an attractive force in the horizontal plane, as predicted in [128, 129]. Markes and Williams [130] point out that, for open systems, a negative slope in the total electrostatic energy is not necessarily an indication of an attractive force. Rather, from a calculation of the forces, the interaction is found repulsive at all distances.

### *3.2. Attractive forces by wake fields*

The highly charged microparticles in the sheath region lead to a substantial deflection of the ion trajectories, which enter the sheath as a directed supersonic flow according to the Bohm criterion. Coulomb scattering bends the ion trajectories in such a way that a net positive space charge is accumulated in the wake of the particle, the so-called ion focus. This effect was predicted on the basis of the dielectric response function by Nambu *et al* [40] and theory was refined later by other authors [41, 42, 125, 131, 132]. Melandsø and Goree studied ion focusing with fluid simulations [126] and by particle simulations [43]. Schweigert *et al* [113] applied Monte-Carlo simulations that include ion-neutral collisons and derived the resulting forces to compare with experiments [32]. Molecular dynamics simulation of ion focusing is now possible in full three-dimensions [133]. While all these models are capable to explain a general, attractive interaction from the positive charge in the wake, there are substantial differences in the distribution of this charge. Complex interference patterns are found to form in collisionless models [131] whereas a single ion focus is found in simulations for the collisionless [126, 133] and collisional case [113].

Wake-field attraction was shown to explain the vertically aligned structure found in the two-layer plasma crystals [32, 134, 135]. Moreover, it was also noted that attraction via wake

fields is inherently asymmetric [32, 113]. A particle can only exert an attractive interaction to another particle, which is downstream from its position but not vice versa. This apparent violation of Newton's third law is introduced by the supersonic ion flow. Nambu *et al* [40] pointed out that wake-field attraction resembles Cooper pairing by the exchange of polarons. Here, the exchange 'particles' are ion-acoustic waves, which can only propagate downstream the supersonic ion flow. Hence, it is the supersonic flow that introduces the symmetry breaking in the interaction forces.

The direct experimental verification of this asymmetric wake-field force was given by studying the attractive forces between two particles of slightly different mass [127, 136]. These particles are suspended at different equilibrium heights in the sheath of an rf discharge and are free to move in their respective equilibrium plane. Without external forcing, these particles tend to form a vertically aligned pair ('dust molecule'). It was found that the vertical alignment disappears at high neutral densities, which can be understood by observations in particle simulations, in which the ion focus is destroyed by an increasing number of charge exchange collisions [113].

The asymmetry of the wake-field force becomes evident, when the upper particle is pushed by the radiation pressure of a focused diode laser (690 m; 30 mW). At low pressure, the lower particle follows the motion of the upper particle and the attractive force can be determined quantitatively from the Epstein friction acting on the lower particle and the horizontal lag between the particles (figure 3(*b*)). When the lower particle is pushed by the focused laser, the aligned pair is disrupted and the upper particle is not found to follow the motion of the lower particle. This observation is in agreement with particle manipulation experiments in plasma crystals [137], where it was found that the entire chain of vertically aligned particles follows the motion of the manipulated top particle, while the chain is disrupted, when a particle in middle of the chain is pushed with the focused laser. Steinberg *et al* [138] report that even two identical particles can attain a vertically aligned position.

The asymmetry of the wake-field forces introduces a novel type of instability (see section 4.7) and has implications for the stability and the melting phase transition of the Coulomb crystal [31–34, 113, 139–141].

### *3.3. Attractive forces by shadowing*

In a finite cloud of microparticles the drag forces by inflowing ions can produce a net attractive force because neighbouring particles make this flow anisotropic [142–144]. This mechanism resembles the effect of *Lesage gravity*, which was intended to explain Newton's gravitational attraction by ether particles hitting the massive bodies randomly but resulting in a net force by mutual geometrical shadowing. This type of net attractive force was not yet observed under laboratory conditions but may play a role in three-dimensional systems of large dust particles, e.g. under microgravity conditions. Fortov *et al* [145] argue that the attractive forces by this mechanism even increase in the presence of a magnetic field.

### *3.4. Coupled oscillations in linear chains*

A linear chain of trapped microparticles can be considered as a system of masses and springs, which is embedded in an additional harmonic potential well due to the confinement. The interparticle spring constant $k$ is given by the second derivative of the interaction potential at the equilibrium distance $b$. Taking the Yukawa type of interaction potential (equation (5)), that

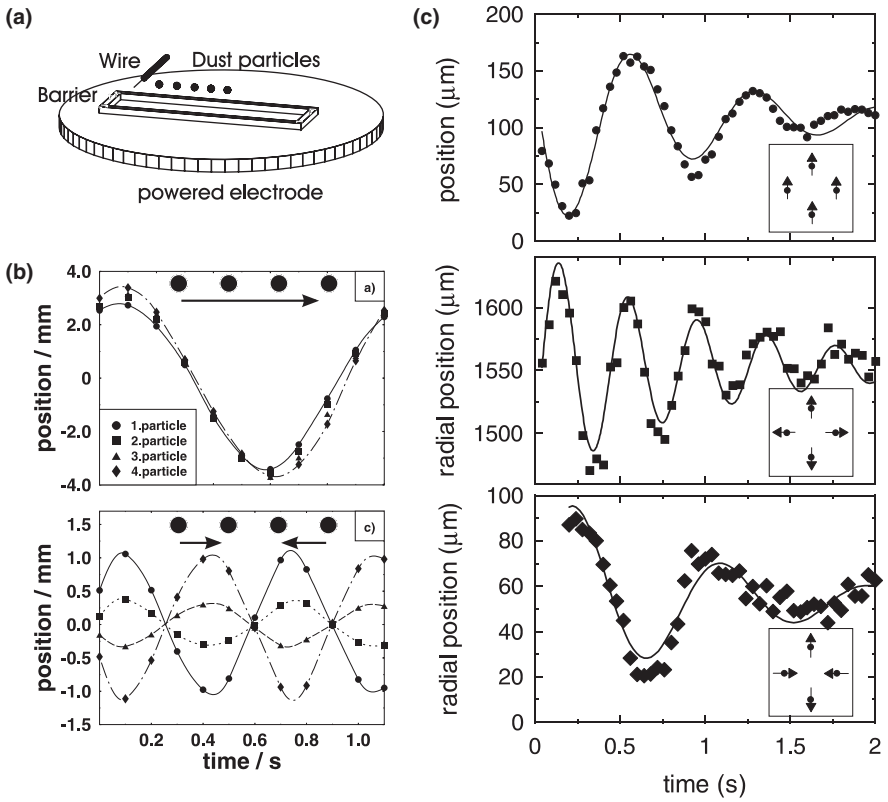


**Figure 4.** (*a*) Trap geometry for a linear chain. (*b*) Coupled oscillations of four particles. Top: sloshing mode, bottom: stretching mode (from [102]). (*c*) Normal modes of the two-dimensional cluster with four particles. Top: sloshing mode, middle: breathing mode, bottom: quadrupole mode (from [146])).

is justified for the interaction perpendicular to the ion flow, $k$ takes the following form

$$k = [2 + 2\kappa + \kappa^2]\frac{Q_{\mathrm{d}}^2}{4\pi\epsilon_0 b^3}\,\mathrm{e}^{-\kappa}, \tag{7}$$

where $\kappa = b/\lambda_{\mathrm{D}}$. Peters *et al* [102] have produced such linear particle chains in an elongated trap geometry (figure 4(*a*)). The oscillations were excited with a biased Langmuir probe at one end of the chain. In a system of four particles, there are four normal modes for this system, the sloshing of all four particles in the confining potential well, two symmetric, and one antisymmetric stretching modes. The eigenfrequency for the lowest symmetrical stretching mode, $\omega_{\mathrm{l}}^2 = [\gamma + (2-\sqrt{2})k]/M_{\mathrm{d}}$ together with the sloshing mode $\omega_{\mathrm{s}}$, can be conveniently used to determine $k$. Figure 4(*b*) shows the sloshing mode (top panel) and the stretching mode in the centre of mass frame (bottom panel). The particle charge results from the vertical resonance and hence, the shielding length $\lambda_{\mathrm{D}}$ can be derived.

This shielding length was under debate [102] and turns out to be different from shielding in the bulk plasma, where $\lambda_{\mathrm{D}} = (\lambda_{\mathrm{De}}^{-2} + \lambda_{\mathrm{Di}}^{-2})^{-1/2} \simeq \lambda_{\mathrm{Di}}$ would be determined by thermal ions. In the sheath, where the particles are suspended, the shielding length is determined by a (diluted) thermal electron population and by non-thermal streaming ions, which are deflected

by the highly charged grains. The shielding length by non-thermal ions can be estimated as

$$\lambda_{\mathrm{Di}}^{\text{non-th}} = \left(\frac{m_{\mathrm{i}}u_{\mathrm{i}}^2}{2\epsilon_0 n_{\mathrm{i}}e^2}\right)^{1/2} = \left(\frac{k_{\mathrm{B}}T_{\mathrm{e}}}{2\epsilon_0 n_{\mathrm{i}}e^2}\right)^{1/2} \simeq 2^{-1/2}\lambda_{\mathrm{De}}, \tag{8}$$

when, in a first step, the ion thermal energy is replaced by the ion streaming energy and, in a second step, the Bohm criterion $u_{\mathrm{i}} = (k_{\mathrm{B}}T_{\mathrm{e}}/m_{\mathrm{i}})^{1/2}$ is applied. Further, ion acceleration in the sheath is neglected, which would reduce the ion density below the electron density at the sheath edge. Hence, the shielding in the sheath becomes electron-like, although it is effected both by electrons and non-thermal ions. As a general finding [102, 103], the shielding strength $\kappa$ was found to take values in the range $\kappa = 1$–$2$.

### *3.5. Normal modes of two-dimensional clusters*

The validity of the presently accepted values for the particle charge and the shielding length can be tested by analysing the normal modes of more complex objects. Melzer *et al* [15] have recently performed experiments on the normal modes of two-dimensional Coulomb clusters in a parabolic trap. Such clusters arrange in regular shells [147–149]. Clusters with up to 100 particles were produced experimentally [150] and their structure compares well with the predictions [148,151]. Radial oscillations of the particles forming small clusters can be excited by a sudden transition from a state with reduced rf power, which increases the interparticle distance, to normal operation. The particles then perform damped oscillations until they reach their equilibrium positions. As an example, some of the normal modes of a four-particle cluster are: (1) the sloshing motion in the confining potential, (2) a *breathing* mode, where all particles move radially, and (3) a quadrupole deformation (figure 4(*c*)). The eigenfrequencies of these modes were determined by rearranging the measured trajectories of the four particles into the eigenvectors, which were then fitted by damped harmonic functions. From the analysis of the eigenmodes, the charge and the shielding length can be derived, which compare well with the resonance method and with earlier findings [101, 102]. The normal modes of small two-dimensional clusters were also recently discussed by Amiranashvili *et al* [152].

Besides vibrational motion, small two-dimensional clusters possess more complicated types of elementary excitations. The shell structure of the clusters results in configurations for certain particle numbers that are particularly stable against the so-called 'intershell rotation'. One of the most stable configuration is, for example, (1, 6, 12) with 1 particle in the centre, 6 particles in the first shell, and 12 particles in the second shell. The high energy barrier for intershell rotation is due to the commensurate number of particles in the inner and outer shell and the hexagonal shape of the particle arrangement. The neighbouring incommensurate configurations (1, 6, 11) or (1, 7, 12) have a much lower energy barrier.

A relative rotation of the outer shell with respect to the inner shell can be excited by a pair of focused laser beams, that exert a torque on the particles in the outer shell [153]. The particles of the inner shell are inhibited by frictional forces with the neutral gas. In a cluster of the (1, 6, 12) configuration the inner shell strictly co-rotates with the outer shell, while the (1, 7, 12) configuration shows differential rotation at different angular velocities. This behaviour demonstrates that the energy barrier for intershell rotation is different for these two cases. A second observation corroborates this view. Under applied laser torque, the (1, 6, 12) configuration can perform a spontaneous structural transition to (1, 7, 11), which leads to the immediate stop of the rotation of the inner shell particles. The co-rotation is resumed as soon as the configuration changes back to (1, 6, 12). Comparing with Monte-Carlo simulations, it could be demonstrated [153] that for Yukawa-type interaction the structural change is energetically favoured over the intershell rotation, which explains the observed behaviour of the (1, 6, 12) cluster.

## 4. Low-frequency electrostatic waves and instabilities in complex plasmas

In complex plasmas, the microparticles influence plasma waves in three different aspects. The large inertia of the particles introduces new electrostatic wave types at very low frequencies, such as the DAW [49] and the dust-cyclotron wave (DCW) [154]. The bound electron charge on the particles gives rise to modifications, e.g. of the ion-acoustic mode [154, 155]. These modes are usually found in weakly coupled plasmas. The dynamical variation of the particle charge leads to a new type of kinetic damping [23]. In plasma crystals, which belong to the class of strongly coupled systems, lattice waves (phonons) appear as compressional modes [55] or shear modes [156].

### *4.1. Dust-acoustic wave*

The DAW is described by the dispersion relation [22, 49]

$$\frac{\omega}{\omega_{\mathrm{pd}}} = \frac{q\lambda_{\mathrm{D}}}{(1+q^2\lambda_{\mathrm{D}}^2)^{1/2}}, \tag{9}$$

where $\omega_{\mathrm{pd}} = (Q_{\mathrm{d}}^2 n_{\mathrm{d}}/\epsilon_0 M_{\mathrm{d}})^{1/2}$ is the dust plasma frequency and $q$ the wave number. This wave exists for $\omega < \omega_{\mathrm{pd}}$. For $q^2\lambda_{\mathrm{D}}^2 \ll 1$, this mode behaves like an acoustic wave $\omega \propto q$. A more complete description for the sound speed [13] includes dust thermal effects

$$C_{\mathrm{DAW}} = \left[\frac{\gamma k_{\mathrm{B}} T_{\mathrm{d}}}{M_{\mathrm{d}}} + \frac{n_{\mathrm{d0}}}{n_{\mathrm{i0}}} Z_{\mathrm{d}}^2 \frac{k_{\mathrm{B}} T_{\mathrm{i}}}{M_{\mathrm{d}}} \left(\frac{1}{1 + T_{\mathrm{i}} n_{\mathrm{e0}}/T_{\mathrm{e}} n_{\mathrm{i0}}}\right)\right]^{1/2}. \tag{10}$$

Here, $\gamma = 1$ for isothermal or $\gamma = 3$ for adiabatic particle motion. The DAW is determined by the pressure of dust, electrons, and ions as well as by dust inertia. In this way, it is analogous to ion acoustic waves, which involve the interplay of electron and ion pressure with ion inertia. Recent refinements of DAW theory include Landau damping and viscoelasticity [157] as well as dust charge fluctuations [82, 158]. Winske *et al* [159] have studied DAWs with molecular dynamics and particle-in-cell simulations. Kortshagen [160] suggested to use DAWs as a diagnostic method for nanometre-sized particles.

Experimental observations of DAWs are mostly from moderately coupled dusty plasmas. Low-frequency oscillations in the frequency range of DAWs were reported from a magnetron device by Chu *et al* [26] and later interpreted as DAWs by D'Angelo [51]. Prabhakara and Tanna [161] observed spontaneously excited low-frequency oscillations in a dust containing hot-cathode discharge. The wave structure of DAWs was observed experimentally in current carrying dusty plasmas, such as an anode double layer [52, 90]. In a dc discharge, Thompson *et al* [54] have measured the full dispersion relation (figure 5(*a*)). Fortov *et al* [162] argue that, in their experiments in a striated neon glow discharge, these waves become unstable from the combined action of dust charge variation, ion drift effects, and external charge-dependent forces. The current-driven DAW in a given dc electric field was also discussed by Ostrikov *et al* [163]. Very recently the individual particle motion in the vicinity of a DAW was measured by 'particle image velocimetry' [164]. In all these experiments mentioned, the damping of DAWs [165] could not be observed, because the waves were self-excited by an electric current, which destabilizes the DAW.

### *4.2. DAWs in Coulomb liquids*

The transition of the DAW into the strong coupling regime was theoretically investigated by various authors. Rosenberg and Kalman [167] studied the case of a strongly coupled dusty plasma close to the liquid–solid transition in the frame of the quasilocalized charge

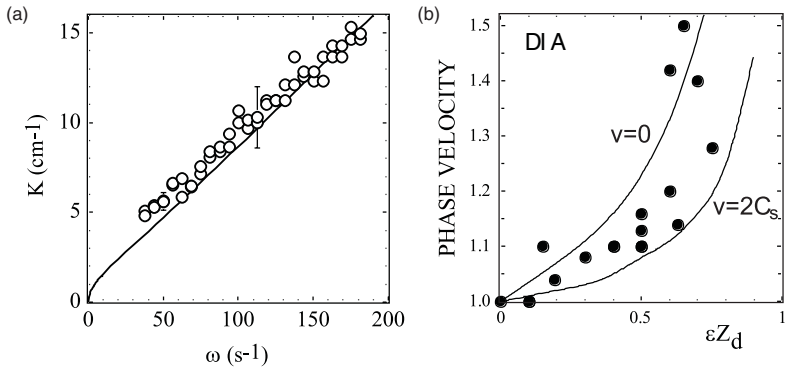


**Figure 5.** (*a*) Dispersion of the DAW measured by Thompson *et al* [54]. (*b*) Phase velocity of DIAW as a function of the electric charge bound to the dust [166]. The solid line corresponds to a non-drifting plasma, the open and filled circles to a plasma drift at $2C_s$.

approximation (QLCA). This system much resembles a disordered solid. It was found that a maximum wave frequency appears, which is lower than the dust plasma frequency. The dispersion curve shows a rollover into backward waves with a group velocity that opposes the phase velocity. Otani *et al* [168] have given an analytical expression for a dust compressional wave, which asymptotically approaches the DAW (DLW) in the weak (strong) coupling limit.

Compressional waves in a strongly coupled Coulomb liquid were studied experimentally by Pieper *et al* [53]. The measured dispersion curve is compared with an extension of the model of Rao *et al* [49] that includes collisional damping of the DAW.

Kalman *et al* [169] have extended their earlier model [167] to include shear modes, which can exist in a strongly coupled Coulomb liquid because of the short-range correlations [170]. The existence of shear waves distinguishes strongly coupled Coulomb liquids from ordinary liquids, which can only support compressional waves. Ohta and Hamaguchi [171] compare molecular dynamics simulations with the QLCA [167] and find a long wavelength cut-off of these shear waves, which is absent in the QLCA [169]. Such shear waves in strongly coupled Coulomb liquids were observed in recent experiments by Kaw [172].

### *4.3. Dust ion-acoustic wave*

A different type of wave appears at higher frequencies, $\omega > \omega_{pd}$, the dust ion acoustic mode (DIAW), with a dispersion relation [154, 155]

$$\omega = \frac{q\lambda_{De}\omega_{pi}}{(1+q^2\lambda_{De}^2)^{1/2}}, \tag{11}$$

which for $q^2\lambda_{De}^2 \ll 1$ reduces to $\omega = qC_s$ propagating at a modified ion-acoustic velocity

$$C_s = \left(\frac{n_{i0}}{n_{e0}}\right)^{1/2}\left(\frac{k_B T_e}{m_i}\right)^{1/2}. \tag{12}$$

The dust influences the wave dispersion through the reduction of free electron charge. This effect was demonstrated experimentally by Barkan *et al* [166] in a Q-machine plasma. At constant dust density, the electron density was gradually reduced until up to 80% of the electron charge was bound to the dust grains. The ion density and the free electron density were determined from the ion and electron saturation currents of Langmuir probes. It is found that, for reduced free electron density, the phase velocity increases over its value in a dust-free

plasma (figure 5(*b*)). For experiments in single-ended Q-machines, the influence of an axial drift has to be taken into account.

### *4.4. Lattice wave modes in plasma crystals*

Plasma crystals are strongly coupled complex plasmas with a (mostly) hexagonal structure in the horizontal plane [30, 31, 34]. Like in real solids with crystalline order, two types of phonons exist in the bulk material [156], the compressional (longitudinal) [55] and the shear (transverse) lattice wave [173]. In a one-dimensional crystal with Yukawa-type interaction, the dispersion relation for the compressional wave reads as

$$\frac{\omega^2}{\omega_{\mathrm{pd}}^2} = \frac{1}{\pi}\sum_{l=1}^{\infty}(2 + 2l\kappa + l^2\kappa^2)\,\frac{\mathrm{e}^{-\kappa}}{l^3}\,\sin^2\left(\frac{qlb}{2}\right). \tag{13}$$

For large $\kappa$, only nearest neighbour interaction has to be taken into account and the familiar dispersion of compressional phonons in solids $\omega \propto \sin(qb/2)$ is recovered. The sound speed $c_{\mathrm{L}}$, $c_{\mathrm{T}}$ for the longitudinal and transverse DLW, respectively, can be written (in the absence of damping and thermal effects) as [156, 173, 174]

$$c_{\mathrm{L,T}} = \lim_{q\to 0}\frac{\partial\omega_{\mathrm{L,T}}}{\partial q} = \lim_{q\to 0}\frac{\omega_{\mathrm{L,T}}}{q} = \left(\frac{Q_{\mathrm{d}}^2}{4\pi\epsilon_0 M_{\mathrm{d}} b}\right)^{1/2} c_{\mathrm{L,T}}^*(\kappa). \tag{14}$$

The factor $c_{\mathrm{L,T}}^*$ is a normalized sound speed for longitudinal and transverse waves in two-dimensional systems, respectively, which depends only on the screening strength $\kappa$:

$$c_{\mathrm{L}}^*(\kappa) = \left(\sum_R \frac{1}{R}\,\exp(-R\kappa)\left[\frac{15}{8}(1 + R\kappa) + \frac{9}{8}R^2\kappa^2\right]\right)^{1/2}, \tag{15}$$

$$c_{\mathrm{T}}^*(\kappa) = \left(\sum_R \frac{1}{R}\,\exp(-R\kappa)\left[-\frac{3}{8}(1 + R\kappa) + \frac{3}{8}R^2\kappa^2\right]\right)^{1/2}. \tag{16}$$

Here, the sum is over all possible interparticle distances $R = r_{ij}/b$ in a hexagonal lattice.

The compressional DLW has a sound-wave-like dispersion $\omega = c_{\mathrm{L}}q$ only for finite values of the screening strength ($\kappa > 0$). For pure Coulomb interaction ($\kappa \to 0$), the compressional wave is dispersive for all wave numbers, $\omega \propto \sqrt{q}$ [55, 175] and consequently $c_{\mathrm{L}}^* \to \infty$. In contrast, the shear wave has always an acoustic dispersion, even for pure Coulomb interaction [156, 175].

In one-dimensional or two-dimensional plasma crystals, besides the shear and the compressional mode, transverse waves exist with vertical particle motion [176]. For this wave mode, the vertical confinement in the sheath provides the restoring force. The dispersion relation

$$\omega^2 = \omega_0^2 - \frac{\omega_{\mathrm{pd}}^2}{\pi}\,\mathrm{e}^{-\kappa}(1 + \kappa)\,\sin^2\left(\frac{qb}{2}\right) \tag{17}$$

shows a similarity with optical phonons in ion crystals. This type of transverse wave was observed experimentally by Misawa *et al* [177] and its peculiar backward-wave nature became evident. Takamura *et al* [98] showed that this wave mode can be spontaneously excited at short wavelength $qb \approx \pi$.

### *4.5. Laser-excited DLWs*

The radiation pressure of a focused laser, which is periodically chopped, is a well-suited technique to excite compressional DLWs in plasma crystals. Homann *et al* have developed this

method for linear chains [178] and for two-dimensional single layer plasma crystals [103]. The geometry of the one-dimensional particle trap was sketched in figure 4(*a*). For the excitation of a linear wave front in the two-dimensional crystal, the beam of an $Ar^+$ laser was expanded into a fan with a cylindrical lens and modulated by a chopper wheel. The advantage of the laser excitation over biased wires is that only the first particle of a linear chain or the first row of particles in two-dimensional systems is forced by the laser. In both cases, a DLW is launched, which propagates as a damped wave into the plasma crystal. By analysing the oscillatory motion of all particles in this system, the real and imaginary part of the wave number $q$ could be determined. The wave dispersion is determined by the particle charge $Q_d$, which is contained in $\omega_{pd}$, and the shielding factor $\kappa$. Comparing with the dispersion of the compressional lattice wave for various values of $\kappa$ (figure 6(*a*)) yields $\kappa = 0.8 \pm 0.4$. Note that this technique requires the independent measurement of $Q_d$, e.g. by the vertical resonance method [29].

### *4.6. Shear waves*

Transverse waves in two-dimensional plasma crystals were excited with chopped laser radiation by Nunomura *et al* [179]. An initial shear stress was produced in the crystal by irradiating a narrow stripe of particles that was aligned with the laser beam. The shear waves propagate in a direction perpendicular to this shear stress. Figure 6(*b*) shows the particle velocity vectors after an initial pulse excitation. Using periodical chopping of the laser beam, the dispersion relation was measured and close agreement with Peeters and Wu's [156] shear wave dispersion was found. A simultaneous measurement of shear waves and compressional waves allows to determine $\kappa$, because the ratio $c_T/c_L$ in equation (15) depends sensitively on $\kappa$ [156].

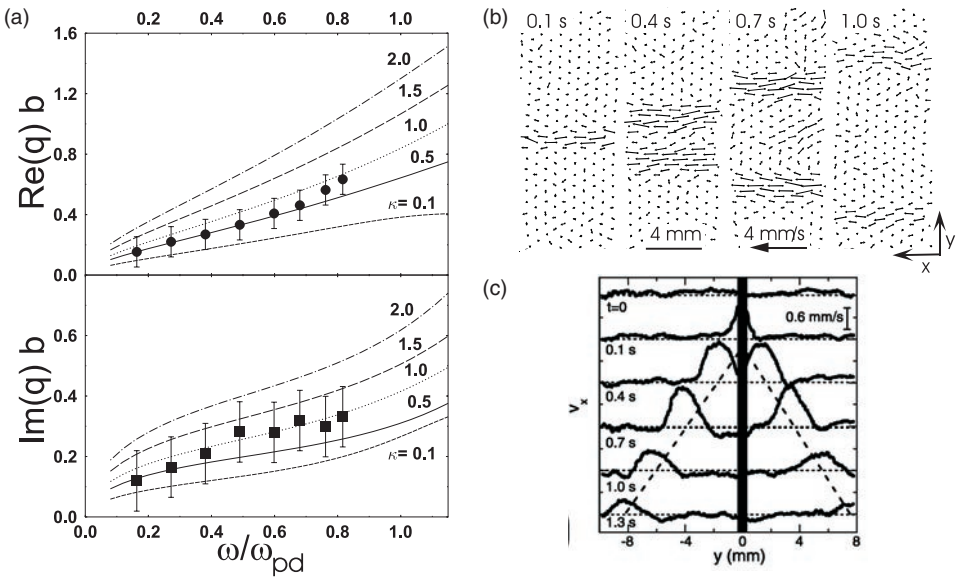


**Figure 6.** (*a*) Dispersion of compressional phonons in comparison with theoretical curves for various values of $\kappa$ (from [103]). (*b*) Propagation of a shear wave in a plasma crystal after pulse excitation. (*c*) Evaluation of transverse particle velocities (from [179]).

### *4.7. Instability by wake-field attraction*

Schweigert *et al* [113] have thoroughly analysed the normal modes in a two-layer plasma crystal. The essence of this model was given before in a simplified analysis using two coupled linear chains of particles [32]. The equations of motion for particles at position $(n)$ in the upper (1) and lower (2) chain read as

$$\ddot{x}_1^{(n)} + \beta \dot{x}_1^{(n)} = \frac{k_1}{M_\mathrm{d}} \left( x_1^{(n-1)} - 2x_1^{(n)} + x_1^{(n+1)} \right) + \frac{A}{d^3}(x_1^{(n)} - x_2^{(n)}), \tag{18}$$

$$\ddot{x}_2^{(n)} + \beta \dot{x}_2^{(n)} = \frac{k_2}{M_\mathrm{d}} \left( x_2^{(n-1)} - 2x_2^{(n)} + x_2^{(n+1)} \right) - \frac{A - A^*}{d^3}(x_1^{(n)} - x_2^{(n)}), \tag{19}$$

where $A$ describes the repulsive interaction between the two chains, which are vertically separated by a distance $d$, and $A^*$ is the (asymmetric) attractive force exerted from the upper chain on the lower. A reduced spring constant $k_2$ is assumed in the lower chain to account for the average attractive force from the neighbouring particle of the upper chain. Because of the symmetry braking by wake-field forces, the dynamical matrix for this system (and for the two-dimensional system considered in [113]) is non-Hermitian, giving rise to unstable waves.

The threshold to instability is defined by a critical friction $\beta^*$. For $\beta < \beta^*$ short wavelength waves with $qb > 1$ become unstable, which have a real frequency close to the dust plasma frequency $\omega_\mathrm{pd}$. In the experiments [31,33], such oscillations were observed below a critical gas pressure and were considered as a precursor for the melting transition of the plasma crystal [31], which converts the ion-streaming energy into oscillatory and eventually random motion of the dust particles. Heating of the ensemble of dust particles by this mechanism was further analysed by Schweigert *et al* in ideal crystals [47,180] and in crystals with defects [140]. In this model, the melting process of the plasma crystal is described as a two-step non-equilibrium phase transition, in which the described instability mechanism sets the system into a hot crystalline state with developed oscillations. At a second lower pressure, the two-dimensional crystal begins to melt. Ivlev *et al* [181] discuss that the the wake-field attraction leads to a coupling of longitudinal and (vertical) transverse waves in a linear chain.

### *4.8. The void instability*

In three-dimensional particle arrangements with nanometric particles [182–184] or with micrometre particles under microgravity [185], a void instability appears: the centre of the bulk plasma is found to be free of dust particles and a sharp boundary between the dust-free and the dust-containing regions is observed. Under some experimental conditions the void was found to rotate around the discharge axis [183, 184] or, in the case of extremely low power a global discharge instability with void size oscillations (*heart beat instability*) sets in. The void formation is due to much more subtle forces than those present in the plasma sheath since the particles are confined in the bulk plasma. An outward directed electric field is established in the void since the ionization rate is enhanced there due to higher electron density. The electric field drives the negative dust into the discharge centre. This inward force is counterbalanced by an outward force, for which the ion drag force is made responsible [186–188]. This effect can be amplified by an ionization instability [184,189]. Due to the different scaling of the outward and inward forces with the particle size, void formation can set in when the particles grow or the discharge conditions are changed. The observed sharp boundary is an effect of the high particle charge [186]. A similar counteraction of forces was recently seen in the experiment of Samsonov *et al* [190], where dust particles in the vicinity of a negatively charged wire are

repelled by the electric field force while those further away are attracted by the action of the ion drag force.

### *4.9. Particle flows in complex plasmas*

There is much experimental evidence that complex plasmas in the fluid state are often characterized by spontaneous flows, e.g. in the melting dynamics [33, 34] or as high speed streams in dc discharges [191]. The processes that lead to these flows are in many cases not well understood, yet.

The situation is different for certain well-defined situations. Rotational motion of plasma crystals is typically observed in magnetized dusty plasmas [19, 192]. In the experiments of Konopka *et al* [192], a permanent magnet produces a vertical magnetic field of $B = 14\,\mathrm{mT}$. The plasma crystal is found to be set into rotation about a vertical axis (the magnetic field direction) by the azimuthal component of the ion drag force. The helium ions are set into rotation by $E \times B$ forces from the radial electrical field from lateral confinement and the vertical magnetic field. The observed rotation at constant angular velocity is compatible with the assumption of a parabolic confining potential. At high values of the applied rf voltage, a reversal of the sense of rotation is seen in the centre of the particle cloud, which is interpreted as a reversal of the radial electric field.

A different geometry of particle circulation is found, when a biased probe is inserted into the complex plasma. Law *et al* [193] observed that a positively biased probe attracts particles, which flow radially inwards in an upper crystal layer and a radial return flow sets in a lower layer. This flow pattern gives a kind of toroidal convection roll around the probe. The sign of the circulation velocity reverses, when the probe is biased negatively.

## 5. Mach cones and nonlinear waves

Mach cones are formed when an object passes through a medium with a velocity $V$ that is greater than the sound speed $c_\mathrm{s}$ of the surrounding medium. At each instant circular wavefronts are excited by the object that superimpose to form a V-shaped Mach cone, which can be most easily observed in a two-dimensional particle cloud. Mach cones in plasma crystals give the unique opportunity to study phenomena of solid-state physics, which are inaccessible in real solids. Up to now, there are only few experimental investigations of nonlinear wave effects in complex plasmas, e.g. shock formation [194, 195], while other phenomena, such as solitary waves [50, 55, 196–202], are still theoretical concepts.

### *5.1. Cone angle and fine structure*

In a dispersionless medium (with $\omega/q = c_\mathrm{s}$), a single Mach cone is formed that obeys the relation

$$\sin\mu = \frac{c_\mathrm{s}}{V} = \frac{1}{\mathcal{M}}, \tag{20}$$

where $\mu$ is the half angle of the Mach cone and $\mathcal{M}$ is the Mach number. Hence, the sound speed in the medium can easily be determined by a measurement of the cone angle. The use of Mach cones as a diagnostic technique was proposed by Havnes *et al* [203] for the dusty plasma in the rings of Saturn. The Cassini spacecraft might observe Mach cones in the rings upon arrival at Saturn in 2004.

Since there are two types of wave modes in plasma crystals, compressional (longitudinal) and shear (transverse) waves, also two types of Mach cones exist, which are distinguished by

the particle motion in the cone front: for the compressional (shear) cone the particles move perpendicular (parallel) to the front.

Dubin [204] has recently presented a theory, in which the dispersive effects in the compressional Mach cone are described by the principle of stationary phase, which is often applied for hydrodynamic waves and for caustic phenomena in optics. Because the group velocity of the compressional DLW is always less than the phase velocity, the interference pattern of all the wavelets excited by the supersonic point source lies inside the Mach cone, which is formed by the extended wave packet that comprises the long wavelength acoustic wavelets. Hence, a main cone is found that still satisfies the Mach cone relation in equation (20) followed by a set of nested secondary cones of decreasing cone angle. The calculated structure shows strong similarity with the multiple Mach cones observed in experiments [174].

### *5.2. Mach cone experiments*

Mach cones have first been observed by Samsonov *et al* [205, 206] by utilizing fast charged particles that, for some unknown reason, move at supersonic speed beneath the actual crystal layer. Due to the electrostatic repulsion these fast particles induce a disturbance in the above crystal layer thus generating compressional Mach cones (figure 7(*a*)). In these experiments it was revealed that at least two distinct nested cones were generated, which were later explained by Dubin [204]. These experiments were, however, restricted by the fact that the direction of the supersonic particles cannot be controlled in the experiment and the supersonic particles are found in a narrow velocity range only.

Melzer *et al* [174] used the focused spot of a laser beam as the supersonic object for the excitation of compressional Mach cones. For this purpose, the laser focus was swept through the crystal by reflection from a tiltable mirror (see inset of figure 7(*b*)). This technique has the advantage that Mach cones can be generated in a reproducible and controlled manner for a broad range of Mach numbers. A large number of identical Mach cone events have been averaged to reveal fine details of the Mach cone structure and indeed up to 4 distinct Mach cones have been observed. In addition, the Mach cone relation (equation (20)) has been verified

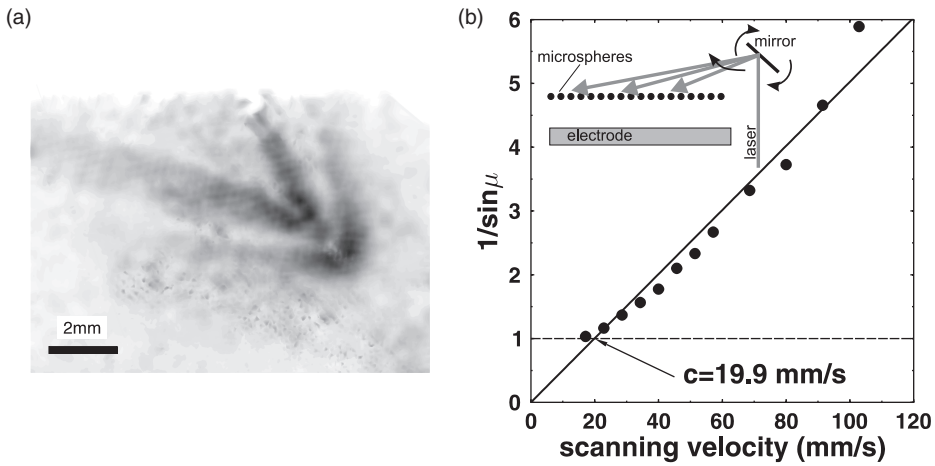


**Figure 7.** (*a*) Compressional Mach cone excited by a fast particle (from Samsonov *et al* [205]). The darkness of the grey shading is a measure for the particle speed $|v|$. (*b*) Cone angle as a function of Mach number for laser-excited compressional Mach cone (from [174]).

for a large range of supersonic velocities from which the sound speed $c_s$ is determined with high accuracy (figure 7(*b*)).

From the sound speed of compressional waves (equations (14) and (15)), the particle charge was found in the range of $Q_d = -6000e$ to $-8000e$ and the screening strength was $\kappa = 1.0 \pm 0.5$. A main difference between the excitation of Mach cones by fast particles and by a laser spot exists. The net momentum transferred to the crystal $\int F \, dt$ is zero in the case of the fast particles and it is finite in the case of the laser due to the particle acceleration in the direction of the beam.

In the experiments of Thompson *et al* [207], where a floating metal wire was moved at supersonic speed through a dusty plasma with sub-micron particles, no Mach cone formation was observed. Rather, the wire left behind a narrow dust-free channel that was rapidly filled in.

### *5.3. Nonlinear wave effects*

Shock formation in ordinary plasmas requires either $T_e \gg T_i$ or other means to reduce Landau damping. Luo *et al* [208] demonstrated that, in a Q-machine plasma with $T_e = T_i$, ion-acoustic shocks could be produced by the addition of negative ions. The reduction of free electrons by attachment to the negative ions has a similar effect on Landau damping. The phase velocity of the wave is found to increase with the reduction of free electrons. A similar effect was observed in the DIAW (section 4.3). The same authors [194] investigated the transformation of DIAWs into shocks in a dusty plasma. For these investigations dust was introduced into the Q-machine plasma. Pulses, which were excited with a mesh grid, showed the expected steepening and the pulse speed was found to increase with the bound electron charge on the dust grains.

Nakamura *et al* [195] have observed DIAW shocks in a double plasma (DP) device. Shock waves in DP devices are usually generated by applying a fast ramp voltage (2 V, 10 $\mu$s risetime) to the source chamber anode. In this way an energetic ion beam of large cross-section is injected into the target chamber. In the absence of dust, the axial density distribution shows formation of an ion-acoustic shock wave with a leading ion bunch and formation of an 'ion phase space hole' on the high-density side of the shock, and subsequent formation of an oscillatory structure on the high-density side. With dust, the steepening of the wave front is also observed, but the oscillatory structure is found to be damped. This damping was attributed to ion–dust friction effects, which can be modelled by the Korteweg–Burgers equation. Ghosh *et al* [209] pointed out that dissipative effects can also arise from non-adiabatic dust charge variation.

## 6. Conclusions and outlook

The examples discussed in this review demonstrate the richness of new dynamical phenomena in complex plasmas, which in many cases have no counterpart in common plasmas. Moreover, with all these particular oscillations and waves it is ensured that the diagnostics of complex plasmas is now in a mature state and a good selection of methods is available to determine the parameters of the charged microparticles and their interaction. The vertical resonance method is suitable to derive the charge-to-mass ratio $Q_d/M_d$ of the particulates. Dispersion and damping of compressional waves in plasma crystals can be used to derive $Q_d$ and the shielding parameter. Alternatively, the ratio of the sound velocities of compressional and shear waves is a sensitive measure for $\kappa$. The analysis of Mach-cone angles also yields the sound velocity, from which the particle charge can be deduced. Laser methods are now widely used to excite oscillations, compressional and shear waves, as well as Mach cones or cluster rotation. Due to the chosen restriction to discuss only such phenomena that have been investigated

experimentally, some important phenomena had to be omitted, such as dust-acoustic solitons (see e.g. [210] and references therein) or many other nonlinear wave phenomena [22].

Complex plasmas in space are always embedded in magnetic fields, which further enrich the dynamical processes, e.g. in terms of dust-Alfvén waves, DCWs and many more, which may be driven by a variety of sources of free energy, like gradients, shear, or electric currents. While there are many theoretical papers in this field (see e.g. [11]), magnetized dusty plasmas are presently nearly unexplored by laboratory experiments.

The field of complex plasmas is also expected to gain many new insights from experiments under microgravity [185, 211]. There, experiments with large particles no longer suffer from sedimentation and the particles are confined in the bulk plasma, where the electric field force is diminished. Moreover, the other weaker forces (ion drag, neutral drag, thermophoresis) become dominant. Oscillations and waves are the natural tools to explore these plasmas. Instabilities, like void formation or heart-beat oscillations, pose challenging questions for the understanding of this new regime of complex plasmas.

## Acknowledgments

One of the authors (A P) thanks DFG for financial support of a sabbatical leave under grant Pi185/21-1. Part of this work was supported by DFG grant Pi185/17-1 and by INTAS grant 97-0775.

## References

[1] Goertz C K 1989 *Rev. Geophys.* **27** 271–92
[2] Northrop T G 1992 *Physica Scripta* **45** 475–90
[3] Selwyn G S, Singh J and Bennett R S 1989 *J. Vac. Sci. Technol.* A **7** 2758–65
[4] Selwyn G S, McKillop J S, Haller K and Wu J 1990 *J. Vac. Sci. Technol.* A **8** 1726–31
[5] Bouchoule A, Plain A, Boufendi L, Blondeau J P and Laure C 1991 *J. Appl. Phys.* **70** 1991–2000
[6] Belenguer P, Blondeau J P, Boufendi L, Toogood M, Plain A, Bouchoule A, Laure C and Boeuf J P 1992 *Phys. Rev.* A **46** 7923–33
[7] Hollenstein C 2000 *Plasma Phys. Control. Fusion* **42** R93–R104
[8] Perrin J, Schmitt J, Hollenstein C and Howling A 2000 *Plasma Phys. Control. Fusion* **42** B353–B363
[9] Bliokh P, Sinitsin V and Yaroshenko V 1995 *Dusty and Self-Gravitational Plasma in Space* (Dordrecht: Kluwer)
[10] Bouchoule A 1999 *Dusty Plasmas: Physics, Chemistry, and Technological Impacts in Plasma Processing* (New York: Wiley)
[11] Verheest F 2000 *Waves in Dusty Space Plasmas* (Dordrecht: Kluwer)
[12] Watanabe Y 1997 *Plasma Phys. Control. Fusion* **39** A59–A72
[13] Merlino R L, Barkan A, Thompson C and D'Angelo N 1998 *Phys. Plasmas* **5** 1607–14
[14] Piel A, Homann A and Melzer A 1999 *Plasma Phys. Control. Fusion* **41** A453–A461
[15] Melzer A 2001 *Plasma Sources Sci. Technol.* **10** 303–10
[16] Liu J M, Juan W T, Hsu J W, Huang Z H and Li I 1999 *Plasma Phys. Control. Fusion* **41** A47–A60
[17] Morfill G E, Thomas H M, Konopka U and Zuzic M 1999 *Phys. Plasmas* **6** 1769–80
[18] Fortov V E, Molotkov V I, Nefedov A P and Petrov O F 1999 *Phys. Plasmas* **6** 1759–68
[19] Sato N, Uchida G, Kaneko T, Shimizu S and Iizuka S 2001 *Phys. Plasmas* **8** 1786–90
[20] Piel A and Melzer A 2001 *Adv. Space. Res.* at press
[21] Shukla P K 2000 *Plasma Phys. Control. Fusion* **42** B213–B221
[22] Shukla P K 2001 *Phys. Plasmas* **8** 1791–803
[23] Melandsø F 1992 *Physica Scripta* **45** 515–20
[24] Melandsø F 1993 *J. Geophys. Res.* **98** 13315–23
[25] Ikezi H 1986 *Phys. Fluids* **29** 1764–6
[26] Chu J H, Du J B and Li I 1994 *J. Phys. D: Appl. Phys.* **27** 296–300
[27] Thomas H, Morfill G E, Demmel V, Goree J, Feuerbacher B and Möhlmann D 1994 *Phys. Rev. Lett.* **73** 652–5
[28] Hayashi Y and Tachibana K 1994 *Jpn. J. Appl. Phys.* **33** L804–L806
[29] Melzer A, Trottenberg T and Piel A 1994 *Phys. Lett.* A **191** 301–8

[30] Quinn R A, Cui C, Goree J, Pieper J B, Thomas H and Morfill G E 1996 *Phys. Rev.* E **53** 2049–52
[31] Melzer A, Homann A and Piel A 1996 *Phys. Rev.* E **53** 2757–66
[32] Melzer A, Schweigert V, Schweigert I, Homann A, Peters S and Piel A 1996 *Phys. Rev.* E **54** R46–R49
[33] Thomas H and Morfill G E 1996 *Nature* **379** 806–9
[34] Thomas H and Morfill G E 1996 *J. Vac. Sci. Technol.* A **14** 501–5
[35] Chiang C and Li I 1996 *Phys. Rev. Lett.* **77** 647–50
[36] Li I, Juan W T, Chiang C H and Chu J H 1996 *Science* **272** 1626–8
[37] Annaratone B 1997 *J. Phys. IV France* **7** C4 155
[38] Farouki R T and Hamaguchi S 1992 *Appl. Phys. Lett.* **61** 2973–5
[39] Dubin D 1993 *Phys. Rev. Lett.* **71** 2753–6
[40] Nambu M, Vladimirov S V and Shukla P K 1995 *Phys. Lett.* A **203** 40–2
[41] Shukla P K and Rao N N 1996 *Phys. Plasmas* **3** 1770–2
[42] Vladimirov S V and Ishihara O 1996 *Phys. Plasmas* **3** 444–6
[43] Melandsø F and Goree J 1996 *J. Vac. Sci. Technol.* A **14** 511–18
[44] Melandsø F 1997 *Phys. Rev.* E **55** 7495–506
[45] Totsuji H, Kishimoto T, Inoue Y, Totsuji C and Nara S 1996 *Phys. Lett.* A **221** 215–19
[46] Totsuji H and Totsuji T K C 1997 *Phys. Rev. Lett.* **78** 3113–16
[47] Schweigert I V, Schweigert V A, Bedanov V M, Melzer A, Homann A and Piel A 1998 *JETP* **87** 905–15
[48] Schweigert V A and Peeters F 1998 *J. Phys.: Condens. Matter* **10** 2417–35
[49] Rao N N, Shukla P K and Yu M Y 1990 *Planet. Space Sci.* **38** 543–6
[50] Verheest F 1992 *Planet. Space Sci.* **40** 1–6
[51] D'Angelo N 1995 *J. Phys. D: Appl. Phys.* **28** 1009–10
[52] Barkan A, Merlino R L and D'Angelo N 1995 *Phys. Plasmas* **2** 3563–5
[53] Pieper J B and Goree J 1996 *Phys. Rev. Lett.* **77** 3137–40
[54] Thompson C, Barkan A, D'Angelo N and Merlino R L 1997 *Phys. Plasmas* **4** 2331–5
[55] Melandsø F 1996 *Phys. Plasmas* **3** 3890–901
[56] Epstein P S 1924 *Phys. Rev.* **23** 710–33
[57] Mott-Smith H M and Langmuir I 1926 *Phys. Rev.* **28** 727–63
[58] Allen J E 1992 *Physica Scripta* **45** 497–503
[59] Allen J E, Annaratone B M and deAngelis U 2000 *J. Plasma Phys.* **63** 299–309
[60] Lampe M, Joyce G, Ganguli G and Gavrishchaka V 2000 *Phys. Plasmas* **7** 3851–61
[61] Barnes M S, Keller J H, Forster J C, O'Neill J A and Coultas D K 1992 *Phys. Rev. Lett.* **68** 313–16
[62] Nitter T 1996 *Plasma Sources Sci. Technol.* **5** 93–111
[63] Spitzer L 1978 *Diffuse Matter in Space* (New York: Wiley)
[64] Lampe M, Gavrishchaka V, Ganguli G and Joyce G 2001 *Phys. Rev. Lett.* **86** 5278–81
[65] Whipple E C 1981 *Rep. Prog. Phys.* **44** 1197–250
[66] Meyer-Vernet N 1982 *Astronom. Astrophys.* **105** 98–106
[67] Whipple E C, Northrop T G and Mendis D A 1985 *J. Geophys. Res.* **90** A8 7405–13
[68] Havnes O, Morfill G E and Goertz C K 1984 *J. Geophys. Res.* **89** 10999–11003
[69] Yamaguchi H and Nejoh Y N 1999 *Phys. Plasmas* **6** 1048–51
[70] Hazelton R C and Yadlowski E J 1994 **22** 91–6
[71] Walch B, Horanyi M and Robertson S 1994 *IEEE Trans. Plasma Sci.* **22** 97–102
[72] Smith M A, Goodrich J, Rahman H U and Mohideen U 2001 *IEEE Trans. Plasma Sci.* **29** 216–20
[73] Barkan A, D'Angelo N and Merlino R L 1994 *Phys. Rev. Lett.* **73** 3093–6
[74] Cui C and Goree J 1994 *IEEE Trans. Plasma Sci.* **22** 151–8
[75] Matsoukas T and Russell M 1995 *J. Appl. Phys.* **77** 4285–92
[76] Matsoukas T, Russel M and Smith M 1996 **14** 624–30
[77] Gordiets B F and Ferreira C M 1998 *J. Appl. Phys.* **84** 1231–5
[78] Gordiets B and Ferreira C 1999 *J. Appl. Phys.* **86** 4118–23
[79] Khrapak S A, Nefedov A P, Petrov O F and Vaulina O S 1999 *Phys. Rev.* E **59** 6017–22
[80] Melandsø F, Bjerkmo Å, Morfill G, Thomas H and Zuzic M 2000 *Phys. Plasmas* **7** 4368–78
[81] Morfill G, Ivlev A and Jokipii J 1999 *Phys. Rev. Lett.* **83** 971–4
[82] Shukla P, Amin M and Morfill G 1999 **59** 389–90
[83] Liebermann M A and Lichtenberg A J 1994 *Principles of Plasma Discharges and Material Processing* (New York: Wiley)
[84] Tomme E B, Annaratone B M and Allen J E 2000 *Plasma Sources Sci. Technol.* **9** 87–96
[85] Tomme E B, Law D A, Annaratone B M and Allen J E 2000 *Phys. Rev. Lett.* **85** 2518–21
[86] Homann A, Melzer A and Piel A 1999 *Phys. Rev.* E **59** 3835–8

[87] Trottenberg T, Melzer A and Piel A 1995 *Plasma Sources Sci. Technol.* **4** 450–8
[88] Arnas C, Mikikian M and Doveil F 1999 *Phys. Rev.* E **60** 7420–5
[89] Fortov V E, Nefedov A P, Torchinsky V M, Molotkov V I, Petrov O F, Samarian A A, Lipaev A M and Khrapak A G 1997 *Phys. Lett.* A **229** 317–22
[90] Thomas E and Watson M 1999 *Phys. Plasmas* **6** 4111–17
[91] Ivlev A V, Sütterlin R, Steinberg V and Morfill G E 2000 *Phys. Rev. Lett.* **85** 4060–3
[92] Zafiu C, Melzer A and Piel A 2001 *Phys. Rev.* E **63** 066403
[93] Schollmeyer H, Melzer A, Homann A and Piel A 1999 *Phys. Plasmas* **6** 2693–8
[94] Nunomura S, Misawa T, Ohno N and Takamura S 1999 *Phys. Rev. Lett.* **83** 1970–3
[95] Ivlev A V, Konopka U and Morfill G E 2000 *Phys. Rev.* E **62** 2739–44
[96] Shukla P K 2000 *Phys. Lett.* A **268** 100–3
[97] Nitter T, Aslaksen T K, Melandsø F and Havnes O 1994 *IEEE Trans. Plasma Sci.* **22** 159–72
[98] Takamura S, Misawa T, Ohno N, Nunomura S, Sawai M, Asano K and Kaw P K 2001 *Phys. Plasmas* **8** 1886–92
[99] Samarian A A, James B W, Vladimirov S V and Cramer N F 2001 *Phys. Rev.* E **64** 025402
[100] Konopka U, Ratke L and Thomas H M 1997 *Phys. Rev. Lett.* **79** 1269–72
[101] Konopka U, Morfill G E and Ratke L 2000 *Phys. Rev. Lett.* **84** 891–4
[102] Peters S, Homann A, Melzer A and Piel A 1996 *Phys. Lett.* A **223** 389–93
[103] Homann A, Melzer A, Peters S, Madani R and Piel A 1997 *Phys. Rev.* E **56** 7138–41
[104] Barnes M S, Colter T J and Elta M E 1987 *J. Appl. Phys.* **61** 81–9
[105] Lapenta G and Brackbill J U 1997 *Plasma Sources Sci. Technol.* **6** 61–9
[106] Lapenta G 1998 *Physica Scripta* **57** 476–80
[107] Lapenta G 1995 *Phys. Rev. Lett.* **75** 4409–12
[108] Lapenta G 1999 *Phys. Plasmas* **6** 1442–7
[109] Manweiler J W, Armstrong T P and Cravens T E 2000 *J. Plasma Phys.* **63** 269–83
[110] Ivlev A V, Morfill G E and Fortov V E 1999 *Phys. Plasmas* **6** 1415–20
[111] Resendes D P 2000 *Phys. Rev.* E **61** 793–800
[112] Mohideen U, Rahman H U, Smith M A, Rosenberg M and Mendis D A 1998 *Phys. Rev. Lett.* **81** 349–52
[113] Schweigert V A, Schweigert I V, Melzer A, Homann A and Piel A 1996 *Phys. Rev.* E **54** 4155–66
[114] Annaratone B A, Khrapak A G, Ivlev A V, Söllner G, Bryant P, Sütterlin R, Konopka U, Yoshino K, Zuzic M, Thomas H M and Morfill G E 2001 *Phys. Rev.* E **63** 036406
[115] Allen J E, Boyd R L F and Reynolds P 1957 *Proc. R. Soc.* A **70** 297–304
[116] Tskhakaya D D and Shukla P K 2001 *Phys. Lett.* A **279** 243–7
[117] Rosenberg M and Mendis D A 1995 *IEEE Trans. Plasma Sci.* **23** 177–9
[118] Rosenberg M, Mendis D A and Sheehan D P 1996 *IEEE Trans. Plasma Sci.* **24** 1422–30
[119] Klumov B A, Popel S I and Bingham R 2000 *JETP Lett.* **72** 364–8
[120] Laframboise J G 1997 *J. Geophys. Res.* **102** 2417
[121] Singh N, Leung W C and Singh G M 2000 *J. Geophys. Res.* **105** 20935–47
[122] Laframboise J G and Sonmor L J 1993 *J. Geophys. Res.* **98** 337–57
[123] Sickafoose A A, Colwell J E, Horanyi M and Robertson S 2000 *Phys. Rev. Lett.* **84** 6034–7
[124] Samarian A A and Vaulina O S 2000 *Phys. Lett.* A **278** 146–51
[125] Vladimirov S V and Nambu M 1995 *Phys. Rev.* E **52** 2172–4
[126] Melandsø F and Goree J 1995 *Phys. Rev.* E **52** 5312–26
[127] Melzer A, Schweigert V and Piel A 1999 *Phys. Rev. Lett.* **83** 3194–7
[128] Resendes D P, Mendonça J T and Shukla P K 1998 *Phys. Lett.* A **239** 181–6
[129] Chen Y P, Luo H, Ye M F and Yu M Y 1999 *Phys. Plasmas* **6** 699–702
[130] Markes M E and Williams P F 2000 *Phys. Lett.* A **278** 152–8
[131] Ishihara O and Vladimirov S V 1997 *Phys. Plasmas* **4** 69–74
[132] Nishimura K 2000 *Phys. Lett.* A **274** 53–8
[133] Maiorov S A, Vladimirov S V and Cramer N F 2000 *Phys. Rev.* E **63** 017401
[134] Joyce G, Lampe M and Ganguli G 2001 *IEEE Trans. Plasma Sci.* **29** 238–46
[135] Hammerberg J E, Lemons D S, Murillo M S and Winske D 2001 *IEEE Trans. Plasma Sci.* **29** 247–55
[136] Melzer A, Schweigert V A and Piel A 2000 *Physica Scripta* **61** 494–501
[137] Takahashi K, Oishi T, Shimomai K, Hayashi Y and Nishino S 1998 *Phys. Rev.* E **58** 7805–11
[138] Steinberg V, Sütterlin R, Ivlev A V and Morfill G 2001 *Phys. Rev. Lett.* **86** 4540–3
[139] Schweigert V A, Bedanov V M, Schweigert I V, Melzer A, Homann A and Piel A 1999 *JETP* **88** 482–91
[140] Schweigert I V, Schweigert V A, Melzer A and Piel A 2000 *JETP Lett.* **71** 58–61
[141] Schweigert I V, Schweigert V A, Melzer A and Piel A 2000 *Phys. Rev.* E **62** 1238–44
[142] Choi S J and Kushner M J 1994 *J. Appl. Phys.* **75** 3351–7

[143] Ignatov A M 1996 *Plasma Phys. Rep.* **22** 648–53
[144] Ignatov A M 1998 *Plasma Phys. Rep.* **24** 677–83
[145] Fortov V E, Nefedov A P and Lakhno V D 1998 *Phys. Lett.* A **250** 149–51
[146] Melzer A, Klindworth M and Piel A 2001 *Phys. Rev. Lett.* **87** 115002
[147] Thomson J J 1904 *Philos. Mag.* **39** 236
[148] Bedanov V M and Peeters F 1994 *Phys. Rev.* B **49** 2667–76
[149] Schweigert V A and Peeters F 1995 *Phys. Rev.* B **51** 7700
[150] Juan W T, Huang Z H, Hsu J W, Lai Y J and Li I 1998 *Phys. Rev.* E **58** R6947–R6950
[151] Lai Y J and Li I 1999 *Phys. Rev.* E **60** 4743–53
[152] Amiranashvili S G, Gusein-zade N G and Tsytovich V N 2001 *Phys. Rev.* E **64** 016407
[153] Klindworth M, Melzer A, Piel A and Schweigert V A 2000 *Phys. Rev.* B **61** 8404–10
[154] D'Angelo N and Song B 1990 *Planet. Space Sci.* **38** 1577–9
[155] Shukla P K 1992 *Physica Scripta* **45** 504–7
[156] Peeters F M and Wu X 1987 *Phys. Rev.* A **35** 3109–14
[157] Murillo M S 2000 *Phys. Rev.* E **62** 4115–19
[158] Xie B S and Yu M Y 2000 *Phys. Plasmas* **7** 3137–40
[159] Winske D, Murillo M S and Rosenberg M 1999 *Phys. Rev.* E **59** 2263–72
[160] Kortshagen U 1997 *Appl. Phys. Lett.* **71** 208–10
[161] Prabhakara H R and Tanna V L 1996 *Phys. Plasmas* **3** 3176–81
[162] Fortov V E, Khrapak A G, Khrapak S A, Molotkov V I, Nefedov A P, Petrov O F and Torchinsky V M 2000 *Phys. Plasmas* **7** 1374–80
[163] Ostrikov K N, Vladimirov S V, Yu M Y and Morfill G E 2000 *Phys. Rev.* E **61** 4315–21
[164] Thomas E Jr and Merlino R L 2001 *IEEE Trans. Plasma Sci.* **29** 152–7
[165] de Angelis U and Shukla P K 1998 *Phys. Lett.* A **244** 557–60
[166] Barkan A, D'Angelo N and Merlino R L 1996 *Phys. Lett.* A **222** 329–32
[167] Rosenberg M and Kalman G 1997 *Phys. Rev.* E **56** 7166–73
[168] Otani N F, Bhattacharjee A and Wang X 1999 *Phys. Plasmas* **6** 409–12
[169] Kalman G, Rosenberg M and DeWitt H E 2000 *Phys. Rev. Lett.* **84** 6030–3
[170] Kaw P and Sen A 1998 *Phys. Plasmas* **5** 3552–9
[171] Ohta H and Hamaguchi S 2000 *Phys. Rev. Lett.* **84** 6026–9
[172] Kaw P K 2001 *Phys. Plasmas* **8** 1870–8
[173] Wang X, Bhattacharjee A and Hu S 2001 *Phys. Rev. Lett.* **86** 2569–72
[174] Melzer A, Nunomura S, Samsonov D and Goree J 2000 *Phys. Rev.* E **62** 4162–76
[175] Bonsall L and Marudin A A 1977 *Phys. Rev.* B **15** 1959–73
[176] Vladimirov S V, Shevchenko P V and Cramer N F 1997 *Phys. Rev.* E **56** R74–R76
[177] Misawa T, Ohno N, Asano K, Sawai M, Takamura S and Kaw P 2001 *Phys. Rev. Lett.* **86** 1219–22
[178] Homann A, Melzer A and Piel A 1996 *Phys. Bl.* **52** 1227–31
[179] Nunomura S, Samsonov D and Goree J 2000 *Phys. Rev. Lett.* **84** 5141–4
[180] Schweigert V A, Schweigert I V, Melzer A, Homann A and Piel A 1998 *Phys. Rev. Lett.* **80** 5345
[181] Ivlev A V and Morfill G 2000 *Phys. Rev.* E **63** 016409
[182] Dorier J L, Hollenstein C and Howling A A 1995 *J. Vac. Sci. Technol.* A **13** 918–26
[183] Praburam G and Goree J 1996 *Phys. Plasmas* **3** 1212–19
[184] Samsonov D and Goree J 1999 *Phys. Rev.* E **59** 1047–57
[185] Morfill G E, Thomas H M, Konopka U, Rothermel H, Zuzic M, Ivlev A and Goree J 1999 *Phys. Rev. Lett.* **83** 1598–601
[186] Goree J, Morfill G E, Tsytovich V N and Vladimirov S V 1999 *Phys. Rev.* E **59** 7055–67
[187] Shukla P K and Morfill G M 1999 *Physica Scripta* T **82** 119–21
[188] Tsytovich V N, Vladimirov S V, Morfill G E and Goree J 2001 *Phys. Rev.* E **63** 056609
[189] D'Angelo N 1998 *Phys. Plasmas* **5** 3155–60
[190] Samsonov D, Ivlev A V and Morfill G E 2001 *Phys. Rev.* E **63** 025401
[191] Thomas E 2001 *Phys. Plasmas* **8** 329–33
[192] Konopka U, Samsonov D, Ivlev A V, Goree J, Steinberg V and Morfill G E 2000 *Phys. Rev.* E **61** 1890–8
[193] Law D A, Steel W H, Annaratone B M and Allen J E 1998 *Phys. Rev. Lett.* **80** 4189–192
[194] Luo Q Z, D'Angelo N and Merlino R 1999 *Phys. Plasmas* **6** 3455–8
[195] Nakamura Y, Bailung H and Shukla P K 1999 *Phys. Rev. Lett.* **83** 1602–5
[196] Bharutram R and Shukla P K 1992 *Planet. Space Sci.* **40** 973–7
[197] Mamun A A, Cairns R A and Shukla P K 1996 *Phys. Plasmas* **3** 702–4
[198] Ma J X, Liu J Y and Yu M Y 1997 *Phys. Rev.* E **55** 4627–33

[199] Tagare S G 1997 *Phys. Plasmas* **4** 3167–72
[200] Xie B S, He K F and Huang Z Q 1998 *Phys. Lett.* A **247** 403
[201] Rao N N 1998 *J. Plasma Phys.* **59** 561–74
[202] Xie B S, He K F, Huang Z Q and Yu M Y 1999 *Phys. Plasmas* **6** 2997–3001
[203] Havnes O, Aslaksen T, Hartquist T W, Li F, Melandsø F, Morfill G E and Nitter T 1995 *J. Geophys. Res.* **100** 1731–4
[204] Dubin D H E 2000 *Phys. Plasmas* **7** 3895–903
[205] Samsonov D, Goree J, Ma Z, Bhattacharjee A, Thomas H M and Morfill G E 1999 *Phys. Rev. Lett.* **83** 3649–52
[206] Samsonov D, Goree J, Thomas H M and Morfill G E 2000 *Phys. Rev.* E **61** 5557–72
[207] Thompson C O, D'Angelo N and Merlino R L 1999 *Phys. Plasmas* **6** 1421–6
[208] Luo Q Z, D'Angelo N and Merlino R L 1998 *Phys. Plasmas* **5** 2868–70
[209] Ghosh S, Sarkar S, Khan M and Gupta M R 2000 *Phys. Lett.* A **275** 109–17
[210] Ivlev A V and Morfill G 2001 *Phys. Rev.* E **63** 026412
[211] Nefedov A P, Petrov O F, Molotkov V I and Fortov V E 2001 *IEEE Trans. Plasma Sci.* **29** 210–15